DEVELOPMENT OF HIGH SENSITIVITY DISTANCE MEASURING FLUIDIC DEVICE

Stephen G. Schneller

A DISSERTAT[redacted]

IN THE

FACULTY OF ENGINEERING

Presented in partial fulfilment of the requirements for
the Degree of Master of Engineering at
Sir George Williams University
Montreal, Canada

April, 1974

DEVELOPMENT OF HIGH SENSITIVITY DISTANCE MEASURING FLUIDIC DEVICE

Stephen G. Schneller

ABSTRACT

A novel, jet-emission type pneumatic linear distance measuring instrument was developed at Sir George Williams University. The sensitivity of the device was established to be in the range of 6×10^{-4} in/psi. The measured distance is the gap between the jet nozzle discharge port and a flat surface. The signal output of the sensor head is negative gauge pressure (vacuum). The range of measurable distance extends over 10^{-3} ins.

A theoretical model was developed to describe the flow phenomenon between the jet nozzle and the opposing surface. Calculated values for signal output using the theoretical model are in good agreement with the experimental measurements.

A standard industrial spray nozzle was adopted with only slight modifications to serve as the sensor head in the experimental set-up. Excellent results were obtained, both in sensitivity and repeatability by this simple device.

ACKNOWLEDGEMENTS

The author wishes to express his gratitude to Dr. C.K. Kwok and Dr. Sui Lin for their guidance and help during the course of the work.

A note of thanks is due to Mr. J. Elliott, who provided invaluable assistance in setting up the test apparatus.

This work was supported by the National Research Council of Canada under Grant No. A 7435.

TABLE OF CONTENTS

CHAPTER 1

INTRODUCTION

page

1.1 Review 1

1.2 The Radial Flow Sensor 9

CHAPTER 2

DESCRIPTION OF APPARATUS AND EXPERIMENTS

2.1 Apparatus 11

2.2 Experiments 13

CHAPTER 3

DESCRIPTION OF FLOW CONFIGURATION

3.1 The Flow Pattern 16

3.2 Analytical Model 19

3.2.1 Choked Flow 19

3.2.2 Calculations of Shock Waves and Shock Front Location 22

3.2.3 Evaluation of Pressure Recovery 24

3.2.4 Results and Discussions 26

CONCLUSION 30

REFERENCES 32

APPENDIX A A-1

APPENDIX B A-8

APPENDIX C A-11

APPENDIX D A-14

NOMENCLATURE

a	-	sonic velocity	ft/sec.
A	-	flow area	in^2
c	-	radius of nozzle chamfer	ins.
c_p	-	specific heat	$ft\text{-}lb/lb^0R$
d	-	nozzle outside diameter	ins.
D	-	hydraulic diameter	ins.
E_f	-	energy loss	in-lb.
g	-	gravitational constant	32.2 ft/sec.^{2}
h	-	flow gap	ins.
l	-	radius of nozzle bore	ins.
m	-	mass flow	lb/sec
M	-	Mach number	
P	-	static pressure	psia.
Q	-	volumetric flow	$in^3/sec.$
r	-	radius	ins.
R	-	radius of annulus	ins.
v	-	velocity	in/sec.
y	-	rv_r dummy variable (from continuity $rv_r=y(z)$)	
γ	-	ratio of specific heats	1.4 for air
ρ	-	density	$slug/in^3$
μ	-	dynamic viscosity	lb sec/in^2
ν	-	kinematic viscosity	$in^2/sec.$

SUBSCRIPTS:	Refer to:
i	point of low pressure measurement
o	nozzle ring outside
s	shock
*	place where M = 1
p^o	total pressure
T^o	total temperature
x	upstream of normal shock
y	downstream of normal shock
1	annulus inside
2	annulus outside
min	smallest value during test run

LIST OF FIGURES

FIGURE		PAGE
1	Auger's Divergent Cone Proximity Sensor	33
2	Le Hunte's Convergent Cone Proximity Sensor	34
3	Sinclair's Three Jet Proximity Sensor	35
4	Modified Air Gauging Apparatus	36
5	S.G.W.U. Back Pressure Sensor	37
6(a)	Radial Flow Test Apparatus	38
6(b)	Sensor Head Details	39
7	Experimental Set-Up	40
8	15 psi Test	41
9	10 psi Test	42
10	Flow Patterns	43
11	Solution of Shock Location	44

CHAPTER 1

INTRODUCTION

1.1 Review

Within the past fifteen years, major developments took place in the field of fluid controls. Following the development of fluidic technology, a wide variety of control devices for industrial and scientific usage was evolved. These instruments, mostly working with air, may offer many advantages over conventional mechanical and electronic control hardware. Among those are, that the three major control functions - sensing, signal computing and activating - can be carried out with the same fluid medium. Fluidic devices are not affected by static electricity and nuclear radiation. They can function at high temperatures where semi conductors are likely to break down.

It is not surprising then, that a concentrated effort is being made to further refine the technology by developing new fluidic control elements.

One particular area of continued interest is in the measurement of linear dimensions. Devices used for this purpose may be classified as "sensing" hardware. Being such, they may either form part of a complete control

system, or they may be used for the sole purpose of instrumentation.

Precision measurement of linear distances is by no means a new art. As early as 1855 Sir Joseph Whitworth developed a machine which facilitated accurate measurements up to 10^{-6}ins. This was followed by the invention of a variety of mechanical instruments, micrometers and the like which utilized Whitworth's screw and wheel-nut principle. Later on various lever magnification techniques were employed for particular measuring requirements. (See Ref. [1]) More recently, optical, electric, electronic and pneumatic devices were added to the already extensive list of instruments. For the purpose of comparison, a brief summary may be offered as follows:

Optical Methods

The apparatus using optical methods could be classified as:

-Microscopes and projectors, which utilize the optical magnification principle.

-Optical comparators and auto-collimators, in which a light beam is deflected on a pivoting mirror. The angular position of the mirror is altered by the measured dimension of an object through mechanical linkages.

-Interferometers, which based on the constant nature of light wave lengths provide absolute linear distance measurements. These devices operate on the principle that light rays which are "in-phase" are additive and rays "out-of-phase" cancel each other. When a condition exists such that the in-phase and out-of-phase relationship between a light bear and its own reflection is repetative, then interference bands of bright and dark areas are produced. The width of the bands (also known as fringes) are the measure of linear or angular position between the prismatic and mirror elements of the apparatus. Suitable linkages cause the relative position of these parts to vary in relation to the measured dimension of an object.

Electric Methods

The electric comparator is operating with two coils which form part of a bridge circuit. When a movable armature between the coils is exactly midway, the bridge is balanced. Through a mechanical linkage the position of the armature can be altered. The resulting unbalance in the bridge circuit is an exact measure of the armature movement. The actuating linkage is positioned by the measured object.

The operation of electronic comparators is based on the alteration of frequency modulation or radio oscillations. An inductance coil and a variable condenser are in combination to form a tuned circuit. When the capacitance of the condenser is changed by varying the air gap between condenser surfaces, the frequency modulation is altered. The adjustment of air gap is effected via a mechanical linkage which in turn is set by the tested object. The frequency modulation is indicative of the measured dimension.

The aforementioned optical and electrical measuring devices are available in a wide range of accuracy. It appears though, that the highest accuracy attainable by either method is one instrument graduation in the order of 10^{-6}ins.

Fluidic Methods

Under the general scope of measuring distances or sensing the positions of objects by fluidic means, many new developments were recorded recently. The devices in existance could be listed in two categories:

A. Proximity sensors, which produce a step-like i.e. digital-pressure signal to indicate the presence of an object within a predetermined distance away from the sensor.

B. Air Gauges, which produce a signal (flow or pressure) that can be calibrated to establish the distance of the object from the sensor. (i.e. the devices produce analogue signals.)

A. Proximity Sensors

In the case of proximity sensors, the usefulness of the devices are enhanced if the object detected can be far away from the sensor head.

Auger (Ref.[2]) reports a sensing distance of 2 ins. with a diverging stream apparatus. In his device, a hollow cone-shaped air jet is issued from a circular nozzle, as shown in Fig. 1. When a flat object is positioned to subtend the flow, a low pressure region is created in the center of the cone. The low static pressure within the cone is measured via an appropriately located pressure tap in the sensor head.

The characteristics of convergent jet proximity sensors were examined by Le Hunte and Ramanathan (Ref.[3]). These investigators obtained very strong step-like signals when an object was placed 0.2 ins. from the sensor head. Their sensor geometric configurations and operating principles are shown in Fig. 3. Basically, the sensor issues a hollow

conical air jet converging into an apex opposite the issuing port. The pressure in the central area is measured. When there is no object placed against the flow, the central core is under vacuum. Next, when an object is brought into close proximity of the head but the apex is still undisturbed, the measured negative pressure remains unchanged. However, when the object is moved to or beyond the apex, the static gauge pressure of the central core switches to positive.

A similar device with three convergent jets were investigated by Sinclair, Letherman and Halford (Ref.[4]). In this case, the maximum distance of an object detectable was found to be 0.4 ins. Sensor geometrics and performance characteristics are shown in Fig. 3. These investigators showed that their apparatus was sensitive to detect the presence of objects with various contours, not only those with flat surfaces subtending the air flow. The dynamic response of the apparatus was also examined by these authors.

B. Air Gauges

Air gauges (or pneumatic distance gauges) are basically comparators, that is, they are calibrated against standard blocks, plugs or rings. The working principle of these

devices is primarily to measure either the back pressure or the quantity of the air flow, which is allowed to escape between the issuing port and the subtending surface of the measured object. Lately, improved sensor designs (Ref. [5]) were introduced, which measure the pressure of a secondary flow generated either around or inside the strong primary flow as shown in Fig. 4.

Commercially available air gauges generally have 0.00005 ins. reading accuracy. It is noted, that owing to their simplicity these instruments are considerably less expensive than optical or electronic devices. Consequently they are favoured in industry wherever they are suitable for a particular application. Due to this commercial acceptance, considerable research effort was made in recent years to further improve the performance of these instruments.

In 1970, a high precision pneumatic distance sensor was developed at Sir George Williams University. The device (shown in Fig. 5) used the ejector principle by measuring the static pressure of the supply air flow before it is issued from a round nozzle.

The sensitivity of this device was observed to be 2×10^{-6} ins. of measured distance variation per mm H_2O

pressure change.* The linearity of the output signal extended over 0.01 ins. range with the closest object-to-sensor distance being 0.005 ins. and the farthest 0.015 ins. While this output characteristic represented improvement of existing air gauges, the repeatability of the measurements fell short of what is required from precision instruments. This was attributed to the fact, that the output pressure was too sensitive to variations in air supply pressure. Nevertheless, the results obtained in accuracy in distance measurements under constant supply pressure were encouraging enough to warrant further investigation and experimentation.

* The mixed units are used deliberately to clearly differentiate between measured distance expressed in British Unit and pressure measurement in mm of water (Metric Unit).

1.2 The Radial Flow Sensor

In an effort to improve the overall accuracy in distance measuring, by pneumatic means, various configurations of sensor heads were evaluated. The one which proved to exhibit the highest sensitivity coupled with good repeatability, shown in Fig. 6, is the topic of this work. For a description of the fundamentals of operation, it is sufficient to say that air is forced to assume a radial flow pattern between the sensor head and the measured object. Since the radial flow velocities decrease with increasing radial distance from the center, a static pressure gradient exists along the radius. At the outward-most periphery of the passage, where the flow exhausts into the surrounding, the static pressure is always atmospheric. With the variation in the flow gap between measured object and sensor head, the radial velocity at a given radius will change for a constant jet supply pressure. As a result, the change in velocity at a pressure tap located within the flow region, produces a change in the measured static pressure with changing flow gap.

An exact relationship between the flow gap width and static pressure readings can be established. It was found that industrial paint spray nozzles could be modified for the

purpose of testing the above described principle.

There are two main functional components in such a spray nozzle: The nozzle itself and a nozzle ring are shown in Fig. 6(a). The nozzle ring is positioned in such a manner that between the two elements, an annular space is formed. The central passage of the nozzle is connected to the air supply. The annular space is used as the pressure tap, the output of which is connected to a manometer.

After investigating a number of different sensor heads of this type, it was found that there are certain relationships between gap width and measured static pressures. However, only a few nozzle and nozzle ring combinations resulted in a geometry which provides a highly sensitive distance measuring device.

It is this particular geometric configuration which will be examined in detail in the following chapters.

CHAPTER 2

DESCRIPTION OF APPARATUS AND EXPERIMENTS

2.1 Apparatus

Fig. 6(a) serves to illustrate the configuration of the sensor head. For the purpose of our experimentation, a Spraying Systems Co. No. 1650 air nozzle was used in combination with #70 ring. The meaning of above designations is as follows:

Nozzle bore (throat)	0.016 ins.
Nozzle outside diameter	0.050 ins.
Nozzle ring hole diameter	0.070 ins.

The only modification performed on the unit was that with the #1650/70 nozzle-nozzle ring assembled, the ring and nozzle surfaces were machined flat, and a chamfer of approximately .004 ins. was cut on the nozzle discharge port. The centrally located nozzle was connected to the constant pressure supply line as shown in Fig. 6(a). The annulus formed between the nozzle outside diameter and nozzle ring inside diameter was used as the pressure tap. Accordingly, the passage under the nozzle ring was connected to one of the legs of a U tube manometer, which

was filled with a liquid of SP. Gr 2.95. Fig. 7 shows the complete experimental set-up. The pressure regulated air supply was passed through a Fisher Porter Mod. FP 1/8 - 16 - G - 5/CD - 10 - 1303 flowmeter using a 1/8 in. diameter stainless steel ball float. The flowmeter exit was connected to the air nozzle as described above. Parallel to the air nozzle a USG Co. pressure gauge of 0-15 psi range was connected. Subtending the nozzle on the test stand was a micrometer graduated in 0.0001 ins.

2.2 Experiments

With the apparatus set up as shown in Fig. 7, the experiments were carried out in the following manner.

A. The nozzle ring was installed on the #1650 nozzle.

B. The reference dimension which co-relates the micrometer readings to the actual distance between the sensor head and plunger end was established.

C. The pressure regulator was set for the required supply pressure. Values of supply pressure were taken on the pressure gauge. i.e. after the flowmeter.

D. The flowmeter reading was recorded, and corrected for the observed back pressure.

E. The micrometer plunger was advanced in steps and manometer readings (one leg only) were taken. After each step, the flowmeter readings were checked.

F. Readings were also taken while retracting the micrometer plunger.

The above described tests were conducted with the pressure set at 10 & 15 psi. Test results are tabulated and shown in Appendix D.

Observations of above tests are plotted on the graphs as follows:

Fig. 8 Nozzle Ring #70
Set Pressure 15 psig

Fig. 9 Nozzle Ring #70
Set Pressure 10 psig

It was observed that at 15 psig test pressure, the flow was 2.74 cu in/sec and at 10 psig, the flow was 2.22 cu in/sec. Both of these stayed constant throughout each individual experiment.

Readings on the micrometer were taken with the aid of a magnifying glass. Accuracy of the readings could be made to within ±1/10 of the calibrated scale. This is equivalent of ±0.00001 ins. reading accuracy for the flow gap.

As can be seen in Figs. 8 & 9, the performance of the sensor may be broken down into three regions. These are identified as A-B, B-C and C-D in Fig. 8. The description of flow configuration throughout the three regions is proposed as follows:

With large values of "h" (Region A-B), the flow entering the radial region is subsonic. When the inlet flow is forced to turn through 90 degrees, a low pressure bubble is formed as shown in Fig. 10(a). The bubble extends over the pressure measuring annulus. As the gap (h) is reduced, the size of the bubble is also reduced. In other words, the effective reduction of the flow area is less than the actual reduction of the flow gap (h). As a result, the sensor does not yield sensitive output.

For a certain value of "h", the attachment point of the jet coincides with the outer edge of the pressure sensing annulus as shown in Fig. 10(b). Further reduction of "h" at that point will cause the flow to enter into the annulus and thus giving a higher pressure reading. Consequently, the measured differential pressure ΔP between the ambient and the sensing annulus is reduced as indicated in the characteristic of Region B-C as shown in Fig. 8. With still further reduction of the flow gap "h", the attachment point finally moves towards the nozzle exit to a new location as shown in Fig. 10(c). From this point on, the device exhibits high sensitivity (Region C-D) in Fig. 8 because the flow is purely radial between the pressure sensing annulus and the exit area.

CHAPTER 3

DESCRIPTION FLOW CONFIGURATION

3.1 The Flow Pattern

In essence the flow path within the sensor has a convergent, a straight and a divergent section. The convergent and straight sections are in the sensor nozzle (see Fig. 6(a)) and their geometry is fixed. The downstream end of the straight section is designated as the throat. The chamfer (Fig. 6(b)) is the first portion of divergent section. The radial flow portion constitutes the last portion of the divergent section. The radial path is of variable width.

Air entering the nozzle is first accelerated in the convergent section. Depending upon the supply pressure, the flow may eventually reach the choking condition at the minimum area which corresponds to the end of the straight section of the nozzle. The flow is then further expanded through the divergent section (chamfer) of the nozzle. Generally, on the divergent portion of the nozzle, a complicated flow pattern occurs involving complex shock and wave patterns and the flow is forced to turn through 90 degrees into the radial passage. For sufficiently

small values of "h", the flow entering the radial passage is supersonic as a result of the expansion after the throat. However, in the section slightly downstream of the throat, it is suspected that a series of oblique shocks take place. Although the multiple shock pattern is highly complex in nature, yet the end conditions across the shock region are very close to that of a normal shock in one dimensional flow. (See Ref. [6]). Therefore, normal shock relationships were used in formulation of the flow model described in the subsequent sections. Downstream of the shock region, the flow is subsonic, and as such, it decelerates toward the outer periphery of the radial passage. It will be shown later that the entire shock region is located upstream of the pressure sensing annulus, therefore, the measured pressure difference ΔP of the sensor output is simply the static pressure recovery between the pressure at the annular region and that of the ambient.

Depending on the supply pressure, the flow may behave in a compressible manner ($M_o > 0.3$) or could be considered incompressible ($M_i < 0.3$) as it passes between the pressure sensing annulus and the exit area. At higher supply pressure, the sensitivity of the device-defined as the ratio of pressure differential ΔP to the variation in gap "Δh" - is better than at low supply pressure. Since in

the test, the highest supply pressure used was 15 psi, in the following detailed analysis, only this condition will be considered. For the 10 psi supply pressure test run, it was calculated that the flow can be considered both laminar and incompressible. The analysis of this test is shown in Appendix A where the solution of the Navier Stokes' Equation for the particular sensor geometry is presented.

3.2 Analytical Model

3.2.1 Choked Flow

The following calculation will serve to show, that during the experiments with the #1650 nozzle and 15 psig supply air pressure the flow was choked in the nozzle.

The measured volume flow was 2.74 in^3/sec. under standard atmospheric conditions. Thus at the point of discharge into the atmosphere, where flow area = $2r_o\pi \times 0.003$ in^2 for h = 0.003 in the average velocity is:

$$\bar{V}_o = \frac{Q}{2\pi r_o h} = \frac{2.74}{0.28\pi \times 0.003} = 1038 \text{ in/sec.} \quad (1)$$

$$\bar{V}_o = 86.54 \text{ ft/sec.}$$

The sonic velocity for air at ambient conditions when temperature = 68°F is: 1117 ft/sec.

therefore the exit Mach number $M_o = \frac{V}{a}$

$$M_o = \frac{86.54}{1117} = 0.0774 \quad (2)$$

From the isentropic flow tables we see that for M = 0.0774

$$A/A^* = 8.0$$

or in other words

$$\frac{A}{A^*} = \frac{2\pi r_o h}{2\pi r^* h} = \frac{r_o}{r^*} = 8 \quad (3)$$

with $r_0 = 0.14$ ins.

$r^* = 0.0175$

r^* is the radius at which the flow would have been choked.

The flow area at $r^* = 0.0175$ is A^*, which is found to be 3.298×10^{-4} in^2

From Fig.6(b), it can be observed that the minimum flow area for the sensor occurs at the end of the straight section of the nozzle. The cross-sectional area A_n at that point is calculated to be $2.01 \times 10^{-4} in^2$. Since A_n is less that A^*, the following conclusions can be drawn:

1. Based on the total flow rate through the sensor element, the flow must be choked.
2. The choked flow must occur at the minimum cross-section area of the flow path, in this case "A_n".
3. Results of the calculation for the theoretical choked flow area A^* to be larger than the actual minimum area A_n indicates that the flow must have undergone some shock processes. Using subscripts x and y to represent conditions upstream and downstream of the shock, and subscript * for choking condition, it can be shown that

$$P_x{}^o A_x^* = P_y{}^o A_y^* \qquad (4)$$

where P_x^0 and P_y^0 are the total pressure upstream and downstream of the shock.

When the flow is choked, the mass flow rate "m" becomes the function of the supply flow total pressure and temperature as shown by Fliegner's Formula

$$m = \frac{\gamma M}{\sqrt{\gamma - 1}} \left(1 + \frac{\gamma - 1}{2} M^2\right)^{-1/2\left(\frac{\gamma+1}{\gamma-1}\right)} \sqrt{\frac{g}{C_p T^0}} \, A P^0 \qquad (5)$$

Under choking condition, M=1, A=A* and since γ=1.4 (Eqn. 5) becomes

$$m = 1.28102 \sqrt{\frac{g}{C_p T^0}} \, A^* P^0 \qquad (6)$$

Assuming the total temperature T^0 to be ambient, the volume flow rate Q can be expressed as

$$Q = 0.104 P^0 \text{ in}^3/\text{sec} \qquad (7)$$

when P^0 is in psi unit.

With an expected upstream pressure variation of not larger than 0.05 psi, this yields maximum 0.3% volume flow variations in the experiments.

3.2.2 Calculation of Shock Waves and Shock Front Location

The following calculations were performed in order to evaluate both the strength and position of the shock for the 15 psi test case. As mentioned previously, the end conditions across multiple shocks may be calculated using normal shock relationships. For estimation of the shock location, flow before and after the shock waves is considered isentropic.

The location of the cylindrical shock front was determined for three values of "h", h = 40×10^{-4} ins., h = 35×10^{-4} ins. and h = 30×10^{-4} ins. by using a graphical method as follows: for each "h" value selected, the exit velocity (at $r = r_o$) and exit Mach number is calculated. Pressure at the exit must equal that of the ambient. Since the velocity is low at the exit, it may be assumed that the temperature is equal to the ambient. A corresponding A/A* is determined using the relationship:

$$\frac{A}{A^*} = \frac{1}{M}\left(\frac{2\left(1 + \frac{\gamma-1}{2} M^2\right)}{1+\gamma}\right)^{1/2} \frac{\gamma+1}{\gamma-1} \qquad (8)$$

At a pre-selected radius, the flow area A_r is used to obtain A_r/A_o. With ratios $A_r/A^* = r/r_o \times A_o/A^*$, Mach number M_r can be determined. This Mach number is denoted as M'_y where subscript y indicates condition downstream of

the shock. From the Normal Shock Tables, the corresponding upstream Mach number M'_x is determined and plotted against the above mentioned pre-selected radius r. A curve can be drawn by using different values of r and calculating the corresponding value of M'_x. Next, the expanding supersonic (and isentropic) flow downstream of the throat is considered. In the radial gap, (diverging path), the Mach number M_x'' is calculated for various values of "r" and plotted accordingly as shown in Fig. 11. The intersection of the curve M_x'' vs. r with M_x' vs. r is then the point of solution for the shock front location.

The process is then repeated for another value of "h". The detailed calculations, presented in Appendix B, yield the following results:

TABLE 1

h	r_s	Mx	My
40×10^{-4}	18×10^{-3}	2.35	.528
35×10^{-4}	20.5×10^{-3}	2.33	.530
31×10^{-4}	23.0×10^{-3}	2.31	.433

3.2.3 Evaluation of Pressure Recovery

Based on the calculations shown in Section 3.2.1 it has been established that the shock occurs well upstream of the pressure sensing annulus region. After the shock, the flow will be subsonic. The pressure difference ΔP between the annulus and the ambient may be calculated by using isentropic flow relationships Eqn. (8) and:

$$\frac{Pi}{Po} = \left(\frac{1 + \frac{\gamma-1}{2} M_o^2}{1 + \frac{\gamma-1}{2} M_i^2}\right)^{\frac{\gamma}{\gamma-1}} \qquad (9)$$

where subscript "i" represents the point where the pressure is measured.

In the actual experiment, the pressure sensing annulus had an outside radius R_2 and inside radius R_1 of 0.035" and 0.025" respectively. The pressure variation between the two extreme radii can be quite significant. Since the actual magnitude of pressure measurement versus distance in the region of interest is quite small, any error introduced in selecting the wrong radius for the point of pressure measurement can be detrimental to the entire analytical exercise.

A force-balance analysis was carried out for the annular region in order to locate the theoretical radius "r_i"

where the pressure should coincide with the average pressure measured in the annular region. Detailed analysis is presented in Appendix C.

It is shown there, that under the specified conditions:

$$r_i = \sqrt{\frac{R_2^2 - R_1^2}{\ln \frac{R^2}{R_1^2}}} \qquad (10)$$

For the above values of R_2 and R_1

$$r_i = 0.0298 \simeq 0.03 \text{ in.}$$

3.2.4 Results and Discussions

Theoretical results based on the model proposed and the compressible flow relationship are presented in the following table and Fig. 8 together with the experimental data.

TABLE 2

$h \times 10^{-4}$	Predicted ΔP Compressible Flow Relationship		Test Measurements	
ins	mm of Liquid (SP.GR=2.95)	psi	mm of Liquid (SP.GR=2.95)	psi
30	172.35	1.444	241	2.020
35	122.34	1.025	143	1.198
40	91.58	0.767	117	0.980

It can be seen, that the trend of theoretical results is the same as that of the observed values. In Fig. 8 between h = 0.0039 ins. and h = 0.0029 ins. the characteristics appear to be nearly linear, and have an average slope of 22 mm of reading (0.1676 psi) per 0.0001 ins. change in distance "h". The 22 mm reading (0.1676 psi) on the test manometer would represent:

$22 \times 2.95 \times 2 = 130$ mm (51.181 ins.) of liquid

column on a reservoir type manometer when filled with fluid of SP.GR = 1.000 (water). In other words, the sensitivity of the sensor is 5.96×10^{-4} in/psi over a range of .001 ins. It can also be seen in Fig. 8 that when the nozzle supply pressure is 15 psig, the measured values of ΔP are higher than the ones obtained by using compressible flow model. In order to account for this discrepancy, it is reiterated that the calculated pressure varies significantly across the pressure sensing annulus. Thus small differences in the selected r_i would result in large differences in the calculated absolute value of ΔP. Sets of calculations for r_i = 0.028 ins. were carried out, and it was found that the calculated values would coincide with measured ones. The theoretical r_i as established in Appendix C is based on the assumption that the flow can be considered incompressible and non-viscous as it passes over the annulus. These may possibly account for the error. A proper correction factor to account for the discrepancies will be most desirable, however, no attempt was made in this work to establish such a correction.

For the purpose of comparison, theoretical results calculated based on the incompressible viscous flow solution shown in Appendix A are also presented in Figs.8 and 9. It can be seen that for nozzle supply pressure of 15 psig, compressible flow model gives better

prediction of the result. However, when the supply pressure is reduced to 10 psig, the viscous laminar flow model correlates better with the experimental results. Initial estimates indicated that the maximum flow Mach number in the region between the annular pressure pick-off and the ambient for the case of 10 psig supply pressure is very much lower than 0.3 for different values of "h". In the case of 15 psig supply pressure, however, Mach number "Mi" exceeds 0.3 when "h" is reduced to approximately 37×10^{-4} in. (Calculation in Appendix B).

It may be concluded that the compressible flow model may be used for cases when the nozzle supply pressures exceed 15 psig. For any supply pressures below that value, incompressible laminar viscous flow solution may be used to predict the sensitivity of the sensor.

It can also be seen from the analysis that better sensor sensitivity can be expected if the radius of the annular pick-off region is reduced. In other words, the annular pick-off should move closer to the nozzle exit, immediately downstream of the shock region.

As mentioned previously that some of the discrepancies occur between the theoretical results and experimental data are due to the selection of wrong "mean radius r_i" of

the annular region. It is believed that the discrepancies can be minimized by reducing the width of the annular pick-off region. By decreasing the gap of the annular region, the region where drop of differential pressure occurred (Zone B-C) as evident in Figs. 8 and 9, will also be correspondingly reduced.

CONCLUSION

A theoretical and experimental investigation of a high sensitivity distance measuring device was presented. Results indicate that the sensor exhibits a sensitivity of 6×10^{-4} in/psi over a range of 10^{-3} ins. The device consists of standard commercially available spray nozzle components manufactured by Spraying System Company with very minor machining modification.

A theoretical compressible flow model was proposed. The flow was first choked and then expanded through a divergent (chamfer) section followed by complex shock patterns. Normal shock relationships were used to approximate the shock process. Downstream of the shock, fluid properties in the subsonic diffusion section were calculated using compressible flow relationships. A graphical method was developed to predict the shock location. Good correlation with experimental data was achieved for cases with nozzle supply pressure of 15 psig.

For lower nozzle supply pressure (P_s<10 psig), a laminar viscous incompressible flow solution of the Navier Stokes Equation was obtained and used to predict ΔP in the diffusion region. Results were compared favourably with

the experimentally measured data.

Trends towards improving the sensor sensitivity were discussed. Narrower annular pick-off should be incorporated in the future sensor element design.

REFERENCES

1. Judge, A. W. — Engineering Precision Measurements, Chapman & Hall Ltd.

2. Auger, R. — A Fluidic Proximity Detector, Third Cranfield Fluidics Conference, Paper E-7, 1968.

3. LeHunte, G.G. & Ramanathan, S. — Development of a Digital Fluidic Proximity Sensor, Fourth Cranfield Fluidics Conference, Paper S-1, 1970.

4. Sinclair, G.G. Letherman, K.M. & Halford, J. — The Static and Dynamic Characteristics of a Reflected Jet Proximity Sensor, Fourth Cranfield Fluidics Conference, Paper S-4, 1970.

5. New Developments in Air Gauging - Machine Shop and Engineering Manufacture - Sept. 1967.

6. Kwok, C. K. — An Experimental Study of Multiple Shocks in a Constant Area Duct, Tech. Note 62-11, McGill University, 1962.

7. Neumann, E.P. & Lustwerk, F. — Supersonic Diffusers for Wind Tunnels, Journal of Applied Mechanics, June 1949.

8. Daily, J.W. & Harleman, D.R.F. — Fluid Dynamics, Addison-Wesley (Canada) Ltd.

9. Moller, P.S. — Radial Flow without Swirl between Parallel Discs, The Acronautical Quarterly, Vol. 14, 1963.

10. John, J.E.A. — Gas Dynamics, Allyn and Bacan.

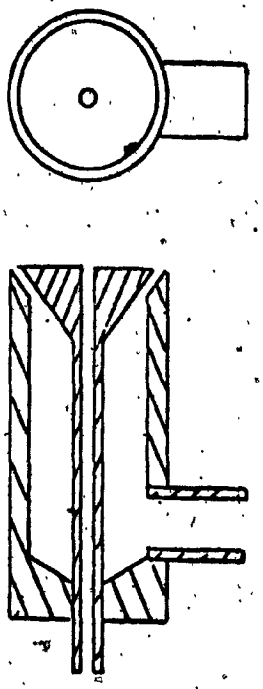

FIG. 1 Auger's Divergent Cone Proximity Sensor

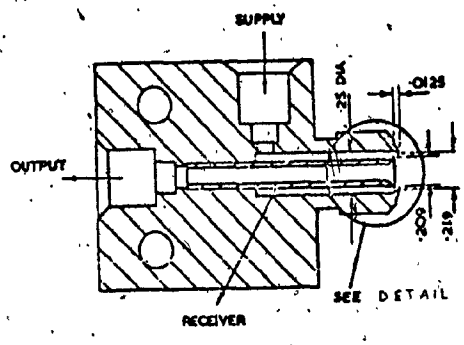

PROXIMITY SENSOR

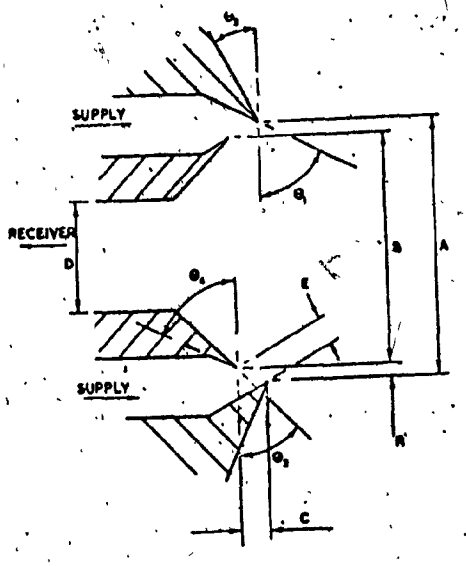

GEOMETRIC VARIABLES OF SENSOR NOZZLE.

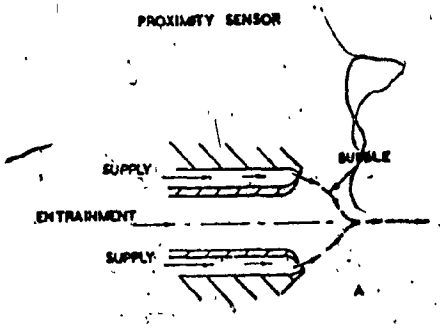

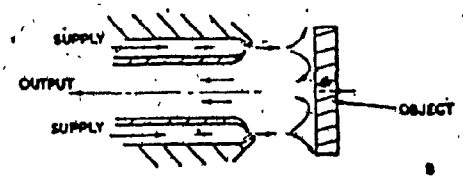

PRINCIPLE OF DIGITAL PROXIMITY SENSOR.

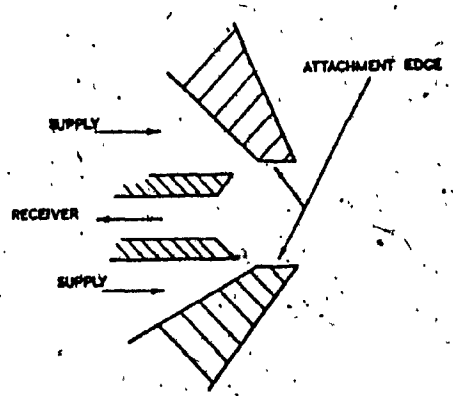

ATTACHMENT EDGE ON SENSOR NOZZLE.

FIG. 2 Le Punte's Convergent Core Proximity Sensor

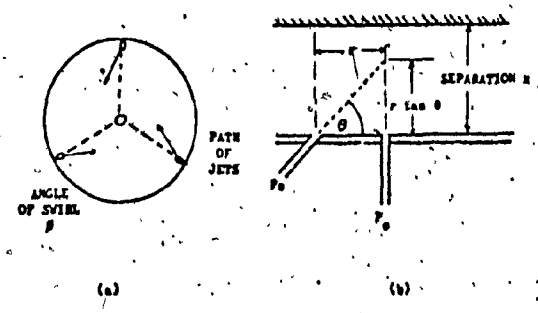

Significant dimensions of the reflected jet proximity detector.

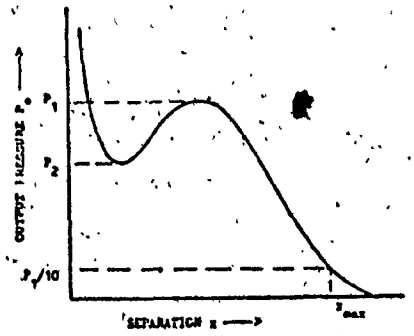

General shape of static characteristic.

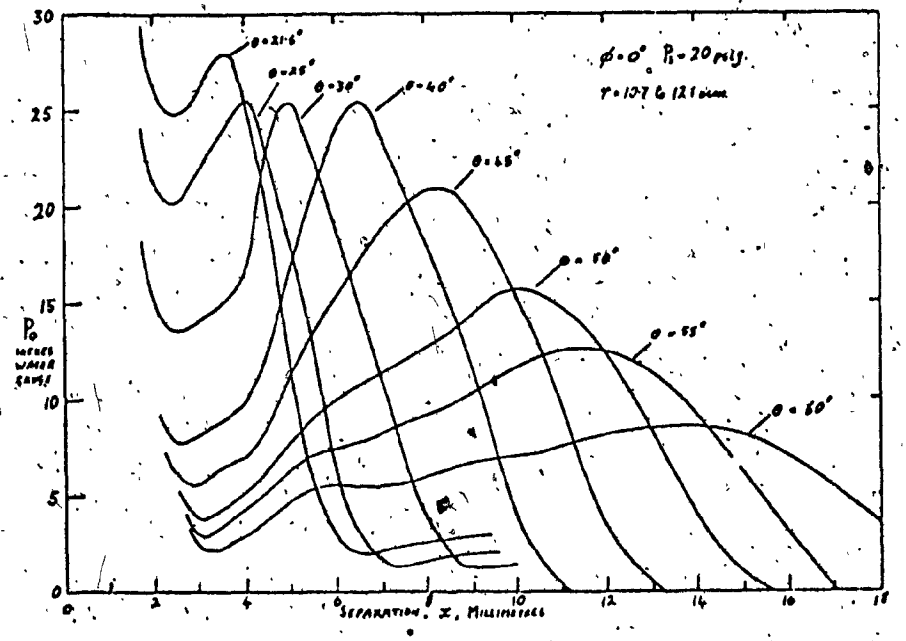

Effect of the angle of inclination of the jets.

FIG. 3 Sinclair's Three Jet Proximity Sensor

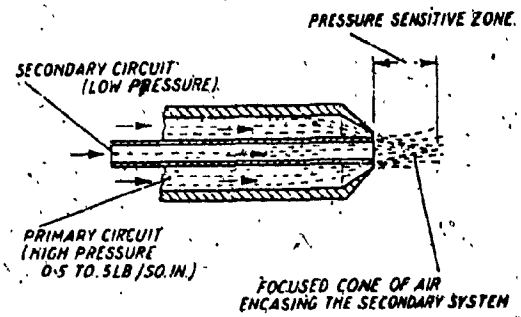

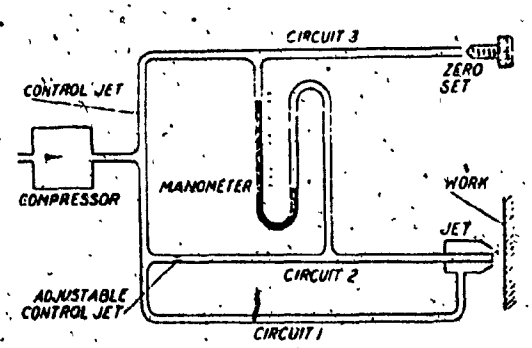

FIG. 4 Modified Air Gauging Apparatus

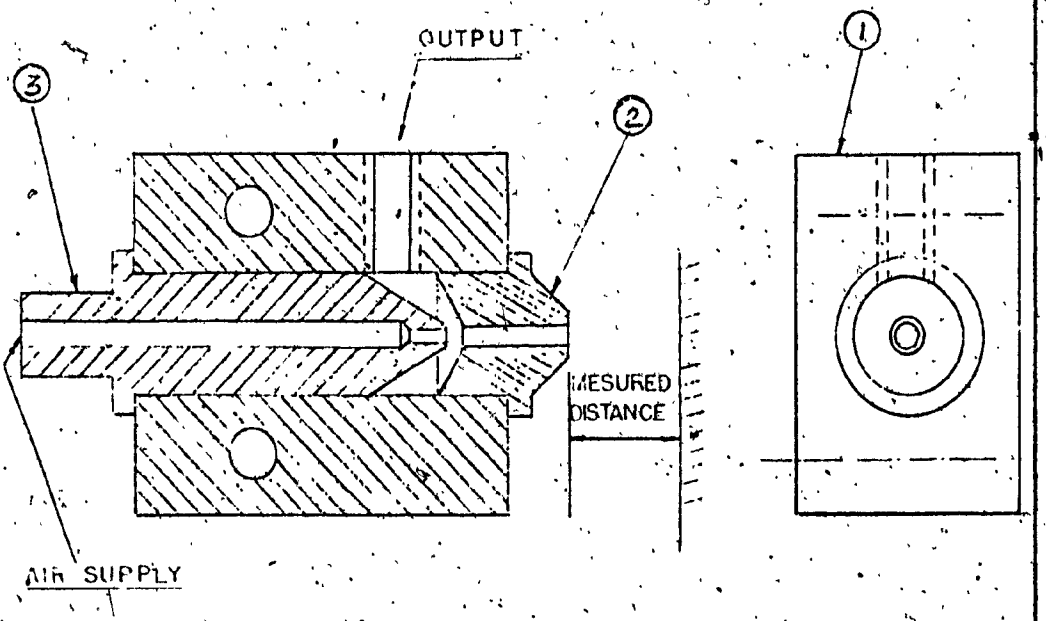

1 BODY

2 RECEIVER NOZZLE

3 EJECTOR NOZZLE

FIG. 5 S.G.W.U. Back Pressure Sensor

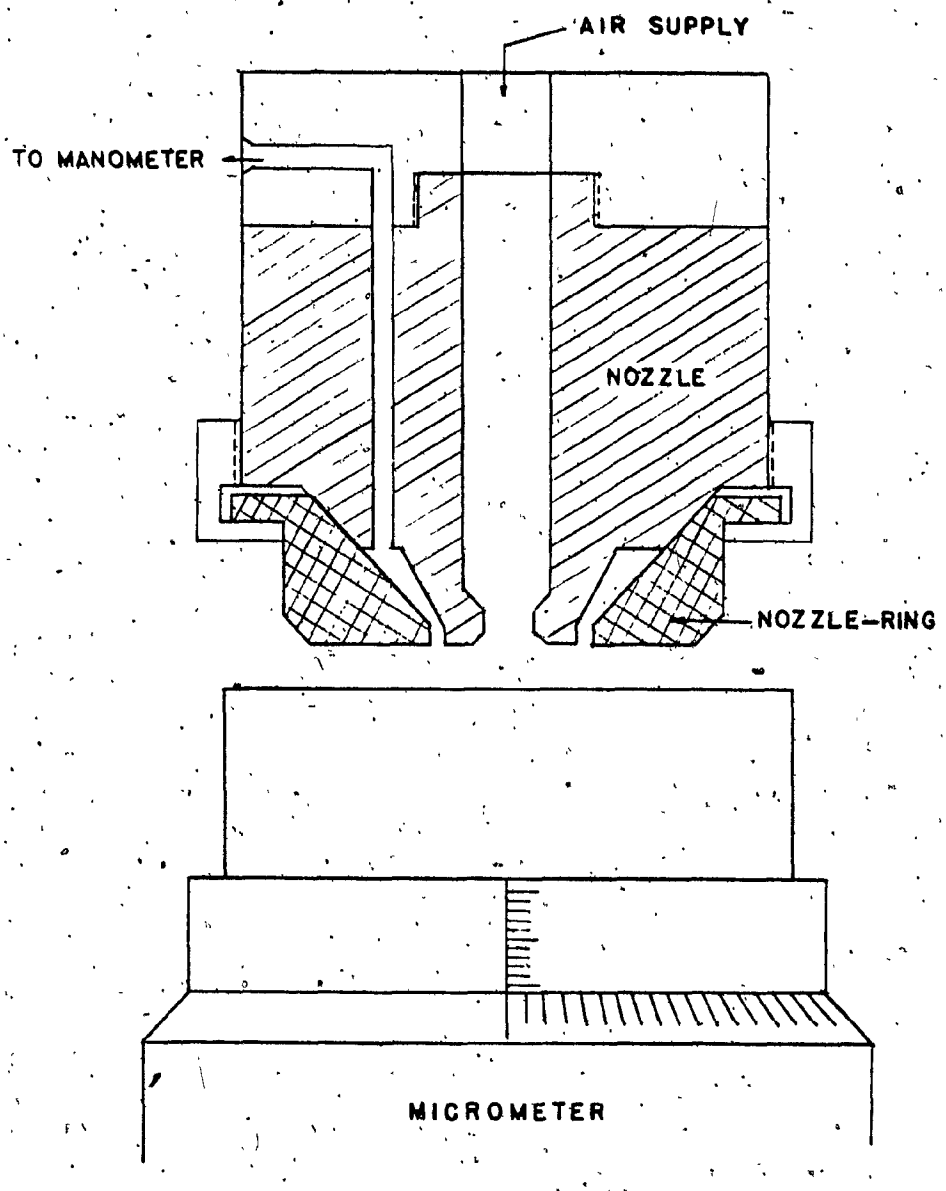

FIG 6(a) RADIAL FLOW TEST APPARATUS

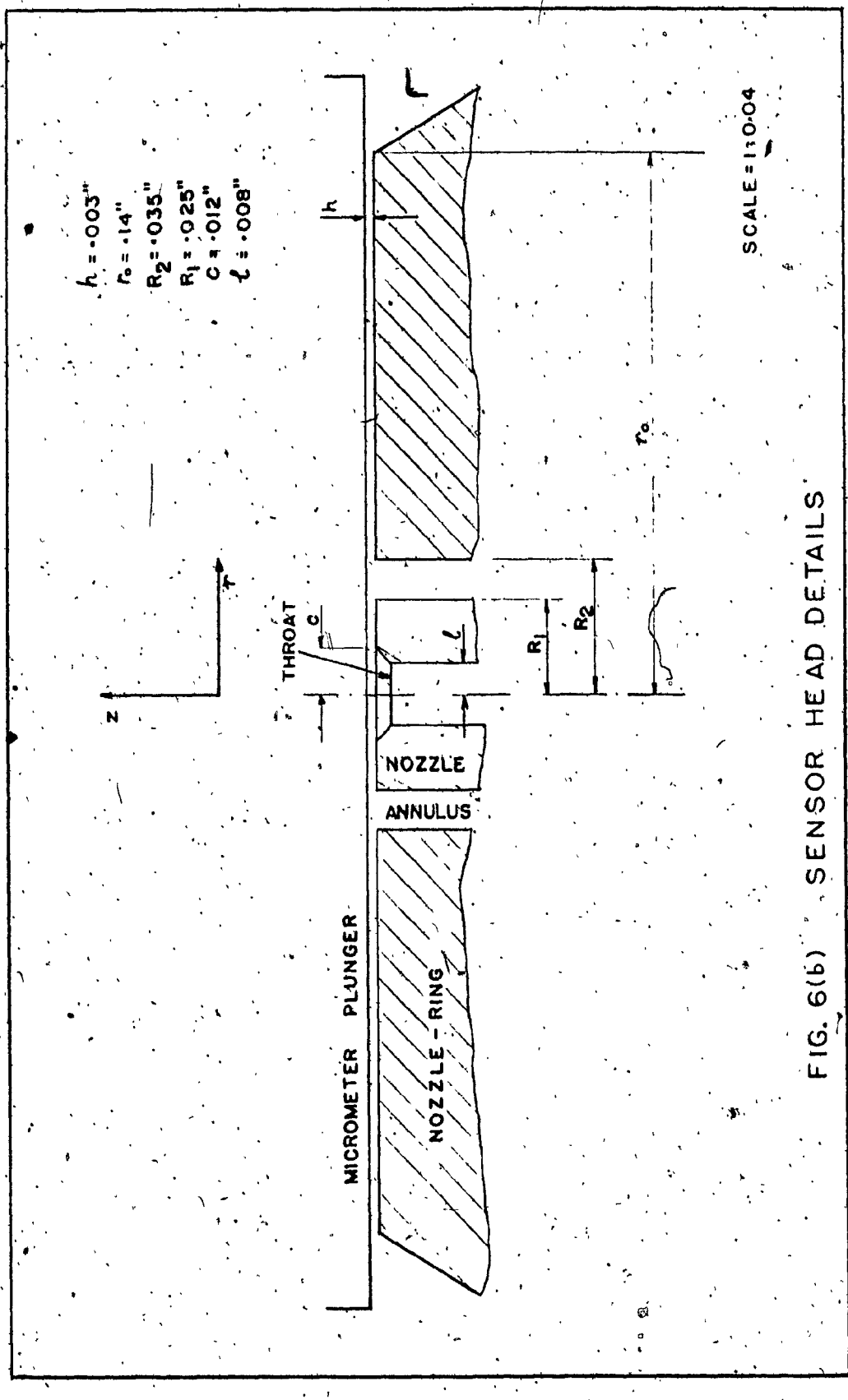

FIG. 6(b) SENSOR HEAD DETAILS

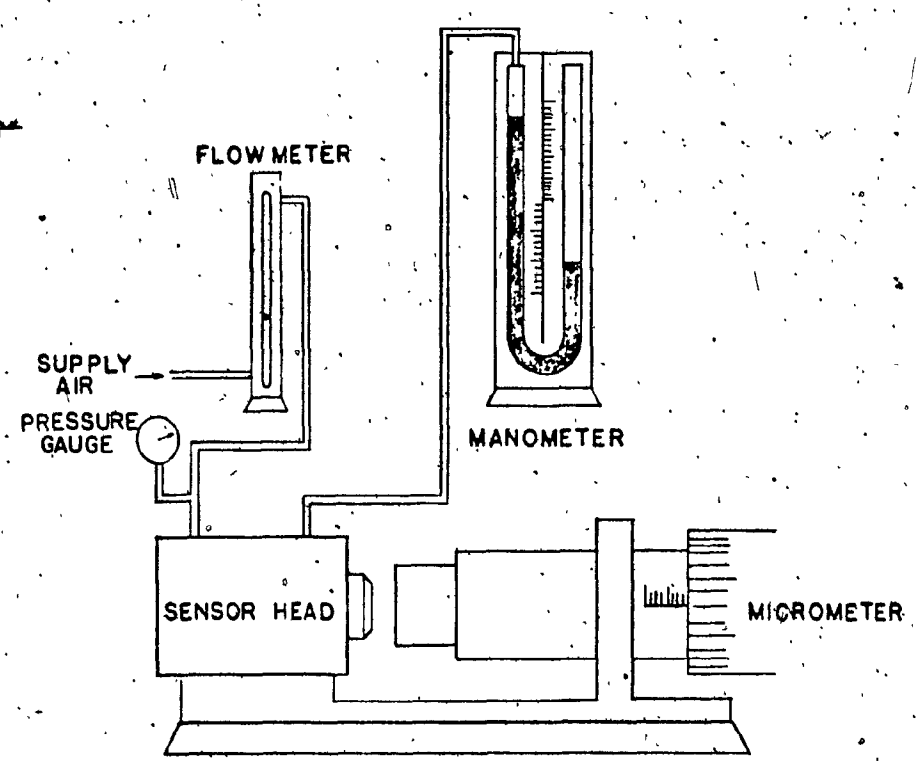

FIG. 7 EXPERIMENTAL SET-UP

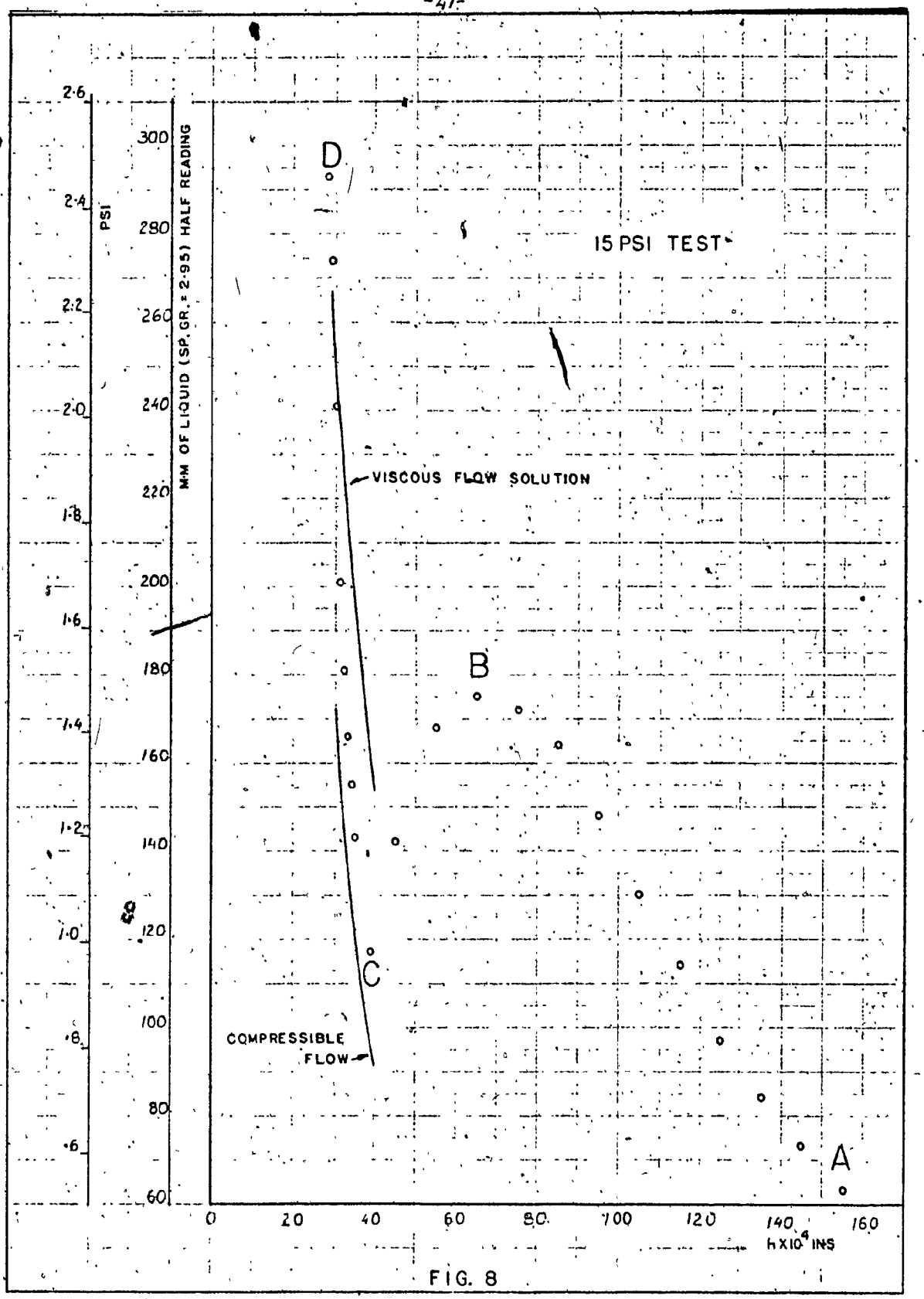
PSI
MM OF LIQUID (SP. GR. = 2·95) HALF READING
2·6
2·4
2·2
2·0
1·8
1·6
1·4
1·2
1·0
·8
·6
300
280
260
240
220
200
180
160
140
120
100
80
60
D
15 PSI TEST
VISCOUS FLOW SOLUTION
B
C
COMPRESSIBLE FLOW
A
0
20
40
60
80
100
120
140
160
h X10⁻⁶ INS

FIG. 8

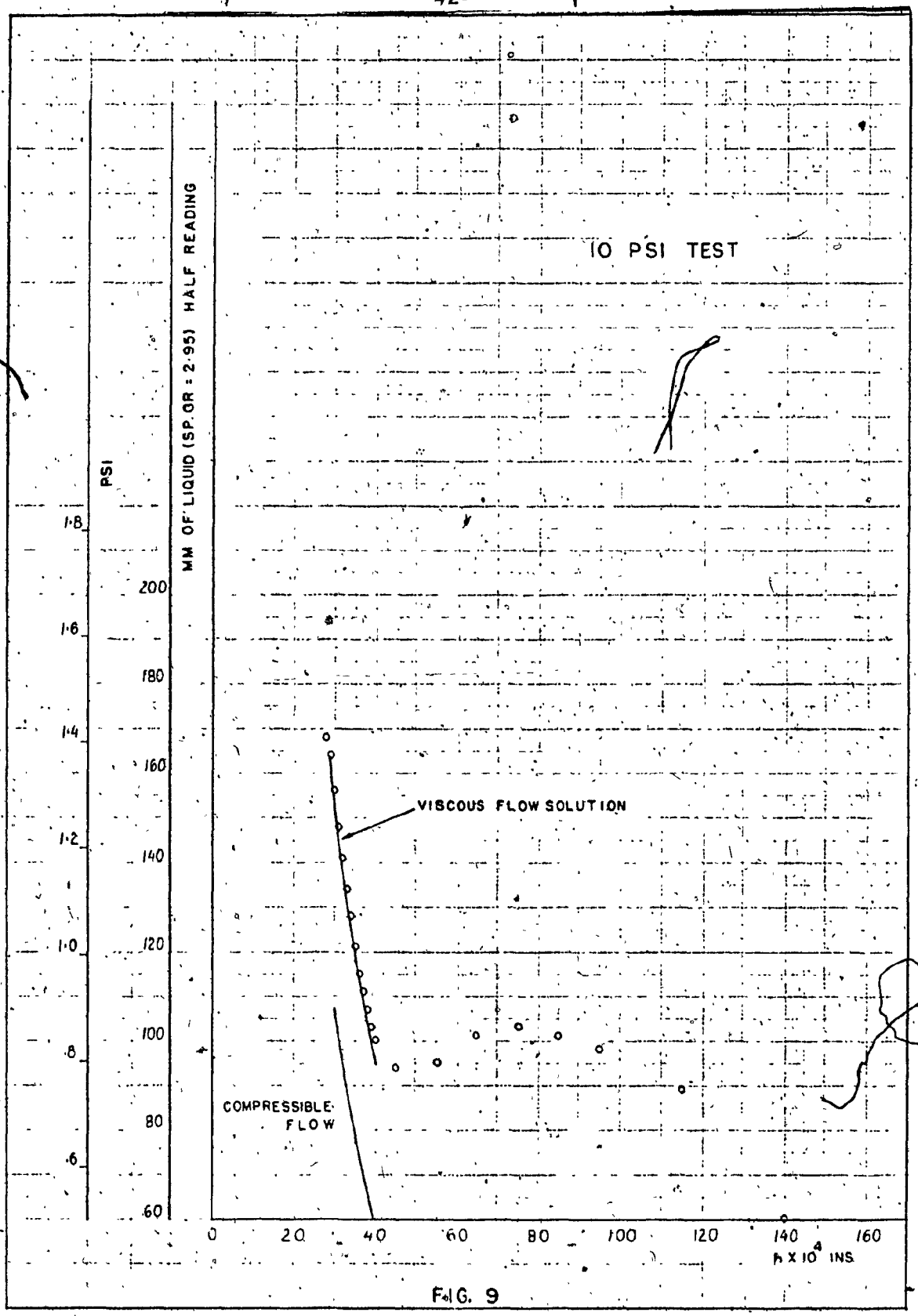
10 PSI TEST
PSI
MM OF LIQUID (SP. GR = 2·95) HALF READING
1·8
200
1·6
180
1·4
160
1·2
140
1·0
120
·8
100
80
·6
60
VISCOUS FLOW SOLUTION
COMPRESSIBLE FLOW
0
20
40
60
80
100
120
140
160
h X 10⁴ INS.

FIG. 9

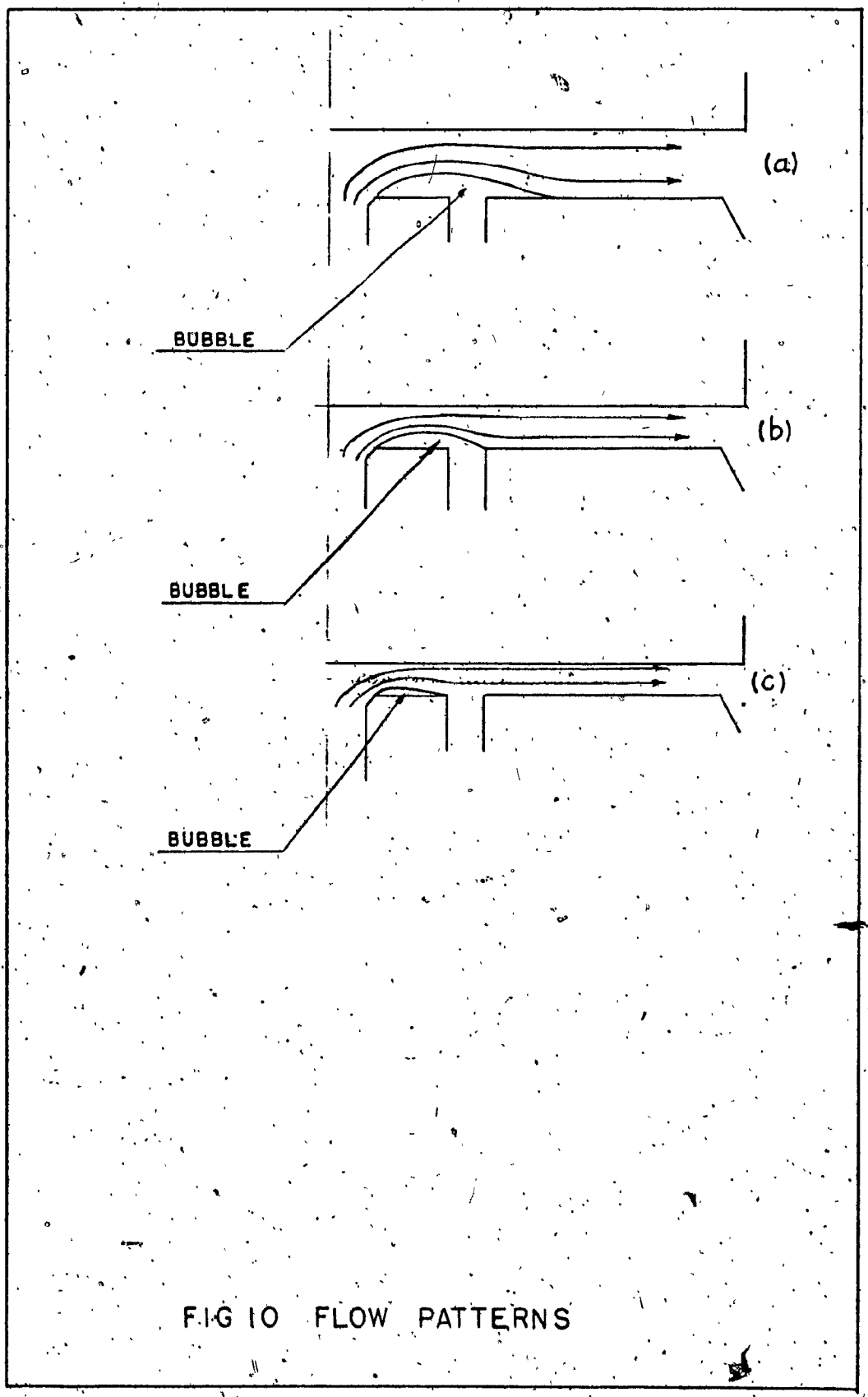

FIG 10 FLOW PATTERNS

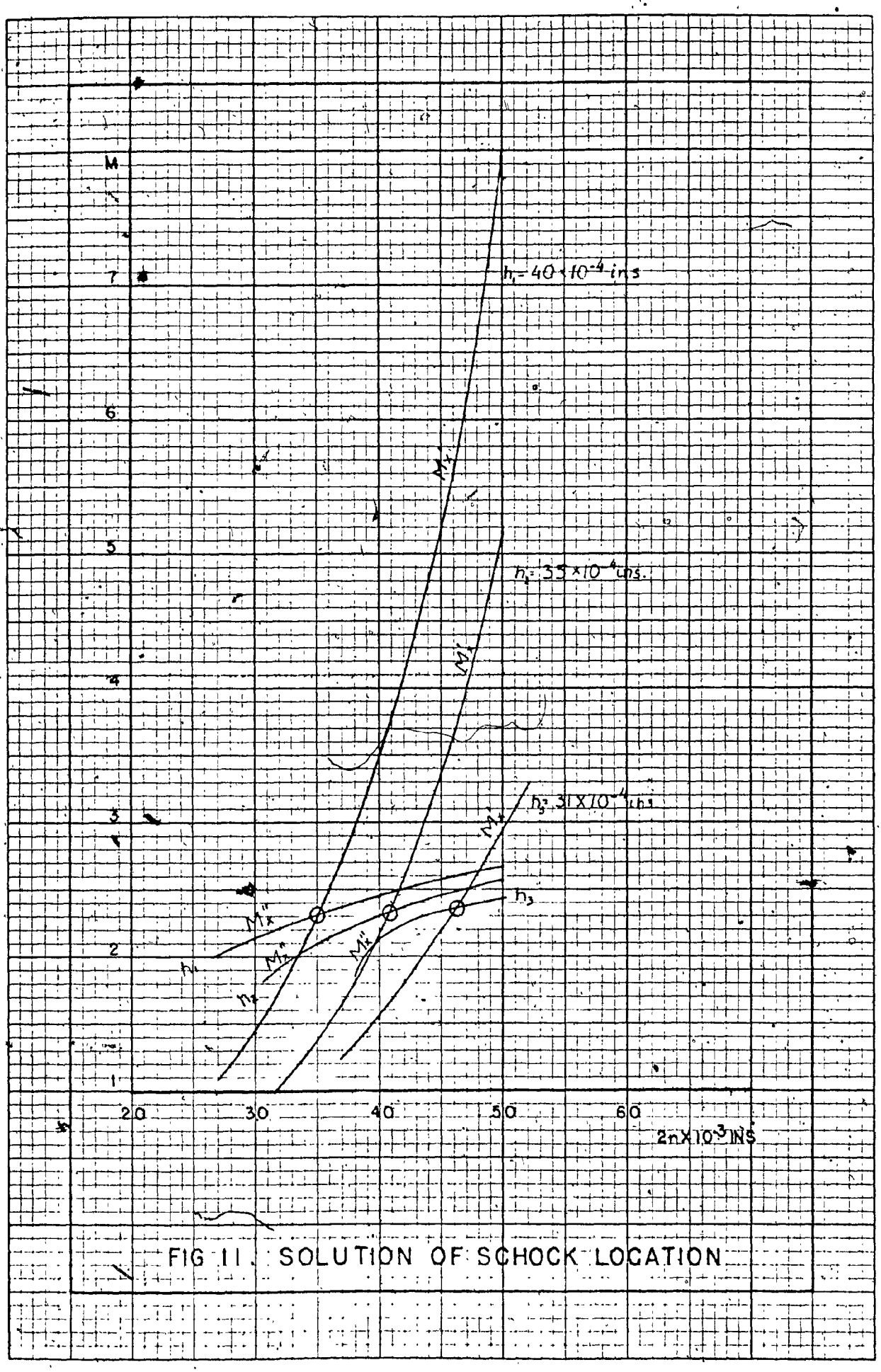

FIG 11. SOLUTION OF SCHOCK LOCATION

APPENDIX A

VISCOUS FLOW SOLUTION

The Navier Stokes equations in the axial (z) and radial(r) direction in cylindrical co-ordinates are:

z Component

$$\rho\left(\frac{\partial V_z}{\partial t} + Vr\frac{\partial V_z}{\partial r} + \frac{V_\theta}{r}\frac{\partial V_z}{\partial \theta} + Vz\frac{\partial V_z}{\partial z}\right) = -\frac{\partial p}{\partial z} + \mu\left(\frac{1}{r}\frac{\partial}{\partial r}\left(r\frac{\partial V_z}{\partial r}\right) + \frac{1}{r^2}\frac{\partial^2 V_z}{\partial \theta^2} + \frac{\partial^2 V_z}{\partial^2 z}\right) + \rho g_z$$

We assume that in the radial flow region Vz and its derivatives are zero. This reduces the above equation to

$$0 = \frac{\partial p}{\partial z} \quad \text{or} \quad p = f(r) \quad \text{(neglecting } g_z\text{)}$$

We conclude that at any radius (r) the pressure is constant across the flow gap. Thus $\frac{\partial p}{\partial r} = \frac{dp}{dr}$

r Component

$$\rho\left(\frac{\partial V_r}{\partial t} + Vr\frac{\partial V_r}{\partial r} + \frac{V_\theta}{r}\frac{\partial V_r}{\partial \theta} - \frac{V_\theta^2}{r} + Vz\frac{\partial V_r}{\partial z}\right) = -\frac{dp}{dr} + \mu\left(\frac{\partial}{\partial r}\left(\frac{1}{r}\frac{\partial [rV_r]}{\partial r}\right) + \frac{1}{r^2}\frac{\partial^2 V_r}{\partial \theta^2} - \frac{2}{r^2}\frac{\partial V_\theta}{\partial \theta} + \frac{\partial^2 V_r}{\partial z^2}\right] + \partial g_r$$

Assuming steady flow and angular velocity $V\theta=0$ this reduces

to $$\rho Vr\frac{\partial V_r}{\partial r} = -\frac{dp}{dr} + \mu\left[\frac{\partial}{\partial r}\left(\frac{1}{r}\frac{\partial [rV_r]}{\partial r}\right) + \frac{\partial^2 V_r}{\partial z^2}\right] \quad (gr=0) \qquad (A.1)$$

The continuity equation in cylindrical co-ordinates is:

$$\frac{1}{r}\frac{\partial (rV_r)}{\partial r} + \frac{1}{r}\frac{\partial V_\theta}{\partial \theta} + \frac{\partial V_z}{\partial z} = 0$$

which, with the above assumptions reduces to

$$\frac{1}{r}\frac{\partial (rV_r)}{\partial r} = 0 \qquad (A.2)$$

Substituting (A.2) into (A.1) we get:

$$\rho Vr\frac{\partial V_r}{\partial r} = -\frac{dp}{dr} + \mu\frac{\partial^2 V_r}{\partial z^2} \qquad (A.3)$$

(A.2) can be expressed

$$\frac{\partial (rV_r)}{\partial r} = 0 = Vr + r\frac{\partial V_r}{\partial r}$$

or $$\frac{\partial V_r}{\partial r} = -\frac{V_r}{r} \qquad (A.4)$$

Again, substituting (A.4) into (A.3) we obtain

$$-\rho\frac{V_r}{r} = -\frac{dp}{dr} + \mu\frac{\partial^2 V_r}{\partial z^2} \qquad (A.5)$$

Integrating (A.2) we obtain

$$r\,Vr = y(z) \qquad (A.6)$$

This expression when differentiated w.r.t.z.

$$r\frac{\partial Vr}{\partial z} = \frac{dy}{dz} \qquad (A.7)$$

$$r\frac{\partial^2 Vr}{\partial z^2} = \frac{d^2y}{dz^2} \qquad (A.8)$$

Substituting (A.7) and (A.8) into (A.5) we obtain the differential equation

$$-\rho\frac{y^2}{r^3} = -\frac{dp}{dr} + \mu\frac{1}{r}\frac{d^2y}{dz^2}$$

$$-\rho\frac{y^2}{r^2} = -r\frac{dp}{dr} + \mu\frac{d^2y}{dz^2}$$

$$\frac{d^2y}{dz^2} = A - By^2 \qquad (A.9)$$

where $A = \frac{r}{\mu}\frac{dp}{dr}$ and $B = \frac{\rho}{\mu r^2}$

The following boundary conditions apply, if z=0 plane is selected to be central in the flow gap.

i) at $z = \begin{Bmatrix} +h/2 \\ -h/2 \end{Bmatrix}$; $Vr = 0$ i.e. $rVr = y = 0$

ii) at $z = 0$; $\frac{\partial Vr}{\partial z} = 0$ i.e. $\frac{dy}{dz} = 0$ (See Eqn.(A.7))

iii) $$\int_{-h/2}^{+h/2} 2\pi rVr\,dz = Q = 2\pi \int_{-h/2}^{+h/2} y\,dz$$

A power series solution for Eqn.(A.9) in the form of

$$y = \sum_{k=0}^{\infty} a_k z^k \quad \text{is assumed}$$

with the first terms expressed as

$$y = a_0 + a_1 z + a_2 z^2 + a_3 z^3 + a_4 z^4 + \ldots \qquad (A.10)$$

Differentiating w.r.t.z yields

$$\frac{dy}{dz} = a_1 + 2a_2 z + 3a_3 z^2 + 4a_4 z^3$$

Applying the second boundary condition we see that $a_1 = 0$

Differentiating again

$$\frac{d^2y}{dz^2} = 2a_2 + 2\times 3a_3 z \quad 3\times 4a_4 z^2 + 4\times 5a_5 z^3 \qquad (A.11)$$

Writing y^2 from Eqn.(A.10) it is seen that the first few terms will be in the form of

$$y^2 = a_0^2 + 2a_0 a_1 z + (a_1^2 + 2a_0 a_2) z^2 + 2(a_0 a_3 + a_1 a_2) z^3 \qquad (A.12)$$

however, knowing that $a_1 = 0$, and comparing the coefficients of z of (A.11) and (A.12) we get $a_3 = 0$. Simple induction will show that all coefficients of odd subscripts are zero. Thus the following results are obtained

$$y = a_0 + a_2 z^2 + a_4 z^4 + \qquad \text{(A.13a)}$$

$$\frac{d^2y}{dz^2} = 2a_2 + 4\times 3a_4 z^2 + 6\times 5a_6 z^4 + \qquad \text{(A.13b)}$$

$$y^2 = a_0^2 + 2a_0 a_2 z^2 + (a_2^2 + 2a_0 a_4) z^4 + \qquad \text{(A.13c)}$$

Comparing the even subscripted coefficients in the differential equation (A.9)

$$2a_2 = A - Ba_0^2 \qquad \text{(A.14)}$$

and

$$3\times 4a_4 = 2a_0 a_2$$

Further even subscripted coefficients will be functions of a_0.

Let us make the approximation that z^4 and higher order terms are negligible.

then $y = a_0 + a_2 z^2$

Making use of the first boundary condition (y=0 at z=h/2)

$$0 = a_0 + \frac{a_2 h^2}{4}$$

or $$a_2 = -\frac{4a_0}{h^2} \qquad \text{(A.15)}$$

Furthermore $$Q = 2\pi \int_{-h/2}^{+h/2} y \, dz$$

$$\frac{Q}{2\pi} = \int_{-h/2}^{+h/2} (a_0 + a_2 z^2) \, dz = a_0 z + \frac{a_2 z^3}{3} \Bigg]_{-h/2}^{+h/2}$$

$$\frac{Q}{2\pi} = a_0 h + \frac{a_2 h^3}{12} \qquad (A.15)$$

Substituting (A.15) into (A.16) we have

$$\frac{Q}{2\pi} = a_0 h + \frac{h^3}{12} \left(-\frac{4a_0}{h^2}\right) = \frac{2}{3} a_0 h$$

$$a_0 = \frac{3}{4} \frac{Q}{\pi h} \qquad (A.17)$$

Substituting (A.17) and (A.15) into (A.14) we obtain

$$-\frac{8a_0}{h^2} = A - B(a_0)^2;$$

$$-\frac{8}{h^2} \times \frac{3Q}{4\pi h} = -\frac{6Q}{\pi h^3} = A - \frac{9}{16} \frac{Q^2}{h^2 \pi^2} B \qquad (A.18)$$

and now re-substituting the coefficients A & B

$$\frac{r}{\mu} \frac{dp}{dr} = \frac{9}{16} \frac{Q^2}{h^2 \pi^2} \frac{\rho}{\mu r^2} - \frac{6Q}{\pi h^3}$$

$$\frac{dp}{dr} = \frac{9}{16}\frac{Q^2}{h^2\pi^2}\frac{\rho}{r^3} - \frac{6\mu Q}{\pi h^3 r} \qquad (A.19)$$

And integrating from r_i to r_o (p_i to p_o)

$$P_o - P_i = \Delta p = -\frac{1}{2} \times \frac{9}{16}\frac{Q^2\rho}{h^2\pi^2}\left[\frac{1}{r_o^2} - \frac{1}{r_i^2}\right] - \frac{6\mu Q}{\pi h^3}\ln\frac{r_o}{r_i}$$

$$\Delta p = \frac{9}{32}\frac{\rho Q^2}{h^2\pi^2}\left[\frac{1}{r_i^2} - \frac{1}{r_o^2}\right] - \frac{6\mu Q}{\pi h^3}\ln\frac{r_o}{r_i} \qquad (A.20)$$

Q = 2.74 in^3/sec at 15 psi supply & 2.22 in^3/sec at 10 psi supply.

ρ = 1.142×10^{-7} slug/in^3

μ = 2.61×10^{-9} lb sec/in^2

ν = 0.02304 in^2/sec

r_o = 0.14 in

r_i = .03 in

Δp (manometer reading) = 119.28 p(psi)

	15 psi Test	10 psi Test
$h \times 10^{-4}$	$\Delta p = \frac{3.1\times10^{-3}}{h^2} - \frac{2.51\times10^{-6}}{h^3}$	$\Delta p = \frac{2.03\times10^{-3}}{h^2} - \frac{2.03\times10^{-6}}{h^3}$
ins	mm of liquid (SPGR=2.95)	mm of liquid SPGR=2.95
24	266	159
30	251	151
35	194	118
38	169	104
40	154.5	95

APPENDIX B

COMPRESSIBLE FLOW CALCULATIONS

1. Measured Flow: A; 15 psi Test.

Reading: 15.1 (Calibrated scale reading)

Corresponding Flow: 1900 $cm^3/min.$

Back Pressure

Correction Factor: 1.42

$$Q = \frac{1900 \times 1.42}{2.54^3 \times 60} = 2.74 \text{ cu}^3\text{sec.}$$

B Similarly for 10 psi Test.

$Q = 2.22 \text{ in}^3/\text{sec.}$

2. Exit Mach Number

Sonic Velocity = 1117 ft/sec. $r_o = 0.14$ ins.

$$M_o = \frac{Q}{2\pi r_o h \times 1117 \times 12}$$

15 psi Test: $M_o = \frac{2.323}{h} \times 10^{-4}$

10 psi Test: $M_o = \frac{1.882}{h} \times 10^{-4}$

3.Graphical Solution for Location of Shock Front.

15 psi Test

Subsonic (exit) region: $\frac{A}{A_o} = \frac{r}{0.14}$; $\frac{A}{A^*} = \frac{A}{A_o}\frac{A_o}{A^*}$

Supersonic region: $\frac{A}{A^*} = \frac{2\pi rh}{\ell^2\pi} = \frac{2rh}{64\times10^{-6}}$

		Subsonic Range						Supersonic Range		
$h\times10^{-4}$	$2r\times10^{-3}$	M_o	A_o/A^*	A/A_o	A/A^*	My'	Mx'	$2r\times10^{-3}$	A/A^*	Mx"
	38			.1358	1.053	.765	1.34	30	1.46	1.81
31	40	.0746	7.827	.1430	1.110	.680	1.56	40	1.94	2.16
	50			.1785	1.385	.478	2.95	50	2.42	2.41
	31.6			.1130	1.000	1.000	1.0	30	1.64	1.97
35	40	.0665	8.800	.1430	1.250	.55	2.18	40	2.19	2.30
	50			.1790	1.560	.41	5.14	50	2.74	2.54
	30			.1072	1.075	.73	1.42	30	1.87	2.12
40	40	.0581	10.030	.1428	1.432	.45	3.5	40	2.50	2.44
	50			.1608	1.610	.40	8	50	3.13	2.68

4. Subsonic Compressible Flow.

$$\Delta p \text{ (psi)} \times 119.28 = \Delta p \text{ (reading)}$$

$$\frac{p_i}{p_o} = \left(\frac{1 + \frac{x-1}{2} M_o^2}{1 + \frac{x-1}{2} M_i^2}\right)^{\frac{\gamma}{\gamma-1}} = \left(\frac{1+0.2M_o^2}{1+0.2M_i^2}\right)^{3.5} \quad ; \quad \frac{A}{A^*} = \frac{1}{M}\left(\frac{1+0.2M^2}{1.2}\right)^3$$

$r_i = 0.03$ ins. $A_i/A_o = 0.2142$

$h \times 10^{-4}$	M_o	A_o/A^*	A_i/A^*	M_i	p_i/p_o	p_i	Δp (psi)	Δp reading	Supply Pressure
30	.0627	9.251	1.981	.3088	.9385	13.77	0.926	107.66	
35	.0537	10.795	2.312	.2607	.9557	14.04	0.6501	77.55	10 psig
40	.0470	12.329	2.641	.2260	.9665	14.20	.4917	58.65	
30	.0774	7.497	1.606	.3952	.9017	13.255	1.445	172.35	
35	.0664	8.738	1.871	.330	.9302	13.67	1.025	122.34	15 psig
40	.0581	9.980	2.137	.284	.9476	13.93	.767	91.58	

APPENDIX C

THE CHOICE OF POINT FOR INSIDE PRESSURE MEASUREMENTS

Let us assume, that the flow above the pressure sensing annulus is non-viscous and incompressible. (Bernoulli's equation applies.)

Let us also assume, that the fluid is static in the measuring duct and that there is force balance existing such that:

$$\int_{R_1}^{R_2} P\, dA = P_i A \qquad \text{(A-21)}$$

Bernoulli's equation for the flow

$$P_o - P = \frac{\rho Q^2}{8\pi^2 h^2}\left[\frac{1}{R^2} - \frac{1}{r_o^2}\right]$$

$$\text{let } \frac{\rho Q^2}{8\pi^2 h^2} = C_1$$

$$P_o - P = \frac{C_1}{R^2} - \frac{C_1}{r_o^2}$$

$$\text{or} \quad P = P_o + \frac{C_1}{r_o^2} - \frac{C_1}{R^2}$$

$$\text{Again let } P_o + \frac{C_1}{r_o^2} = C_2$$

then $p = C_2 - \frac{C_1}{R^2}$ (A.22)

Substituting Eqn.(A-22) into (A-21) and having

$$\int_{R_1}^{R_2} \left(C_2 - \frac{C_1}{R^2}\right) 2\pi R dR = (R_2^2 - R_1^2)\pi p_i \qquad dA = 2R\pi dR$$

$$\pi(R_2^2 - R_1^2)C_2 - 2\pi C_1 \ln\frac{R_2}{R_1} = (R_2^2 - R_1^2)\pi p_i$$

$$C_2 - \frac{C_1 \ln\left(\frac{R_1}{R}\right)^2}{R_2^2 - R_1^2} = p_i \qquad \text{(A.23)}$$

and after resubstituting the constants

$$P_i = P_o + \frac{\rho Q^2}{8\pi^2 h^2 r_o^2} - \frac{\rho Q^2}{8\pi^2 h^2} \frac{\ln\left(\frac{R_2}{R_1}\right)^2}{R_2^2 - R_1^2}$$

$$\Delta P = P_o - P_i = \frac{\rho Q^2}{8\pi h^2} \frac{\ln\left(\frac{R_2}{R_1}\right)^2}{R_2^2 - R_1^2} - \frac{1}{r_o^2} \qquad \text{(A.24)}$$

comparing Eqn.(A-24) with Bernoulli's equation for the average inside radius r_i.

$$\Delta P = \frac{\rho Q^2}{8\pi h^2}\left[\frac{1}{r_i^2} - \frac{1}{r_o^2}\right]$$

we see that

$$\frac{1}{r_i^2} = \frac{\ln\left(\frac{R_2}{R_1}\right)^2}{R_2^2 - R_1^2}$$

$$\text{or } r_i^2 = \frac{R_3^2 - R_1^2}{\ln \frac{R_3^2}{R_1^2}} \qquad (A.25)$$

Employing terminology found in other works we would say that for the inside pressure tap radius square we use the "LOG MEAN RADIUS SQUARE - DIFFERENCE".

Example: for $R_1 = 0.025$ in.

$R_2 = 0.035$ in.

$r_i = 0.0298$ in.

Note: the average: $\frac{R_2 + R_1}{2} = 0.03$ in.

It is duly observed that the above consideration is not valid strictly for viscous flow or compressible isentropic flow. We would venture to say, however, that the error would be small.

APPENDIX D

Experimental Results

	Ps = 15 psig			Ps = 10 psig	
Distance	Run 1	Run 2	Run 3	Run 1	Run 2
in.	mm sp. 2.95	mm sp. 2.95	mm sp. 2.95	mm sp. gr. 2.95	mm sp. gr. 2.95
0.0185	44	43	44	30	
0.0175	50				
0.0165	56				
0.0155	63	61	63		
0.0145	73				
0.0135	84				
0.0125	97				
0.0115	114			78	
0.0105	130	130	132		
0.0095	148	146	150	98	
0.0085	164	162	164	101	
0.0075	172	170	173	102	
0.0065	175	173	176	101	
0.0055	168	164	170	102	102
0.0045	142	136	146	103	
0.0039	117	110	119	107	
0.0035	143	140	145	121	120
0.0034	155	154	156	128	127
0.0033	166	165	166	134	135
0.0032	181	181	180	141	140
0.0031	201	199	202	149	148
0.0030	241	240	241	156	157
0.0029	274	273	274	164	163
0.0028	292	291	292	168	167
0.0027	295	295	296	169	169
0.0026	291	290	290	168	168
0.0030	240	239	241	165	163
0.0040	121	117	123	102	102
0.0050	153	152	153	101	
0.0060	172	171	170	101	